catalysts

MDPI

Article

Theoretical Study on Influence of Cobalt Oxides Valence State Change for C_6H_5COOH Pyrolysis

Si-Mei Fu [1], Yue Zhao [2], Jiang-Tao Liu [2], Wen-Sheng Liang [2], Gang-Sen Li [1], Wei Huang [2,*] and Zhi-Jun Zuo [2,*]

1 College of Chemistry and Chemical Engineering, Taiyuan University of Technology, Taiyuan 030024, Shanxi, China; fusimei@tyut.edu.cn (S.-M.F.); ligangsen@tyut.edu.cn (G.-S.L.)

2 Key Laboratory of Coal Science and Technology of Ministry of Education and Shanxi Province, Taiyuan University of Technology, Taiyuan 030024, Shanxi, China; zhaoyue@163.com (Y.Z.); liujiangtao@163.com (J.-T.L.); liangwensheng@163.com (W.-S.L.)

* Correspondence: huangwei@tyut.edu.cn (W.H.); zuozhijun@tyut.edu.cn (Z.-J.Z.); Tel./Fax: +86-3516018073 (Z.-J.Z.)

Received: 24 January 2019; Accepted: 19 February 2019; Published: 21 February 2019

Abstract: Benzoic acid (C_6H_5COOH) is selected as coal-based model compound with Co compounds (Co_3O_4, CoO and Co) as the catalysts, and the influence of the valence state change of the catalyst for pyrolysis process is investigated using density functional theory (DFT). DFT results shows that the highest energy barrier of C_6H_5COOH pyrolysis is in the following order: $E_a(CoO) < E_a(Co_3O_4) < E_a(\text{no catalyst}) < E_a(Co)$. In general, Co_3O_4 catalyst accelerates C_6H_5COOH pyrolysis. Then, the catalytic activity further increases when Co_3O_4 is reduced to CoO. Finally, Co shows no activity for C_6H_5COOH pyrolysis due to the reduction of CoO to metallic Co.

Keywords: DFT; benzoic acid; catalytic pyrolysis; Co compounds

1. Introduction

Coal pyrolysis is an essential step for coal combustion, gasification, carbonization, liquefaction and so forth. In other words, to achieve the effective utilization of coal, pyrolysis is a significant method in the condition of inert gas [1–3]. With the addition of catalysts, energy consumption is reduced, the production rate is less volatile and the quality of products are improved [1,4]. Therefore, some researchers have studied coal catalytic pyrolysis. Wang conducted experiments and found that K_2CO_3 exhibits a catalytic effect on coal pyrolysis [5]. Fu proposed that metal chlorides KCl, alkali metal CaO, and transition metal Fe_2O_3 promote coal pyrolysis [6]. Some researchers also find that Co compounds improve the catalytic activity, e.g. coal depolymerization and hydrogenation, tar yield and so on [7–10].

The structure of coal is complex and it has undefined molecular compositions [11,12]. Furthermore, the separation of coal and catalysts is difficult after the catalytic pyrolysis reaction, and the effect of the catalyst for coal catalytic pyrolysis is hard to investigate via experiment. Hence, to study the coal catalytic pyrolysis mechanism, some organic compounds were selected as model compounds. It is well known that carboxyl (COOH) is the most common functional groups in coal [13], and aromatic compounds such as benzene (the simplest aromatic) are also common [11]. Therefore, the behavior of COOH group in coal during pyrolysis by using the compounds C_6H_5COOH is modeled by experiment and calculation [12,14–17]. However, those theoretical studies focus on the coal pyrolysis [18,19], and the role of catalysts are not considered. Recently, the role of some catalysts (ZnO, γ-Al_2O_3, CaO, and MgO) for coal catalytic pyrolysis is studied by using DFT, which C_6H_5COOH, C_6H_5CHO and $C_6H_5OCH_3$ are selected as the model compounds [20–22]. It is found that

the catalysts alter the energy barrier and reaction pathway. For example, ZnO, CaO, and MgO catalysts promote C_6H_5COOH decomposition, but γ-Al_2O_3 catalyst causes no catalytic effect on C_6H_5COOH decomposition. However, all the catalysts alter the reaction pathway. In fact, reducing gases are formed such as H_2 and CO during the process of coal pyrolysis [6]. In the case, some unstable catalysts are possibly reduced. For example, it is found that the reduction process of Co_3O_4 under reducing gases is in this order: $Co_3O_4 \rightarrow CoO \rightarrow Co$ [23,24]. What is the influence of the catalyst valence state change for coal catalytic pyrolysis?

To answer the question, benzoic acid (C_6H_5COOH) is selected as a coal-based model compound, and Co compounds (Co_3O_4, CoO and Co) are selected as the unstable catalysts under coal catalytic pyrolysis condition. Then, the effect of the valence state change of the Co-based catalyst for coal catalytic pyrolysis is investigated using DFT.

2. Results and Discussion

2.1. C_6H_5COOH Pyrolysis

As shown in Figure 1, three possible pathways are studied for C_6H_5COOH pyrolysis: $C_6H_5COOH \rightarrow CO_2 + C_6H_6$ (E_a = 2.89 eV, ΔH = -0.05 eV), $C_6H_5COOH \rightarrow C_6H_6COO$ (E_a = 2.78 eV, ΔH = 2.70 eV), and $C_6H_5COOH \rightarrow C_6H_5COO + H$ (E_a = 5.93 eV, ΔH = 5.90 eV). The energy barriers of pathways 1 and 2 are similar, which are far lower than that of pathway 3. Therefore, pathways 1 and 2 for C_6H_5COOH pyrolysis are possible, which is similar with our previous study [20]. The potential energy diagrams of C_6H_5COOH pyrolysis and the corresponding initial states (IS), transition states (TS) and final states (FS) are shown in Figure 2. As shown in Figure 2, the pyrolysis pathways of C_6H_5COOH are $C_6H_5COOH \rightarrow CO_2 + C_6H_6$ and $C_6H_5COOH \rightarrow C_6H_6COO \rightarrow CO_2 + C_6H_6$, which are in accordance with the experimental results [25–27].

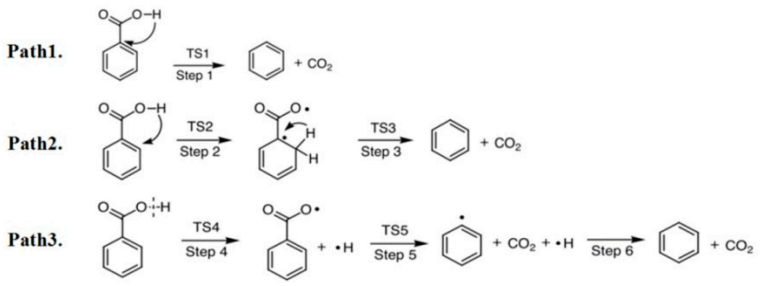

Figure 1. Three pathways for the pyrolysis of C_6H_5COOH.

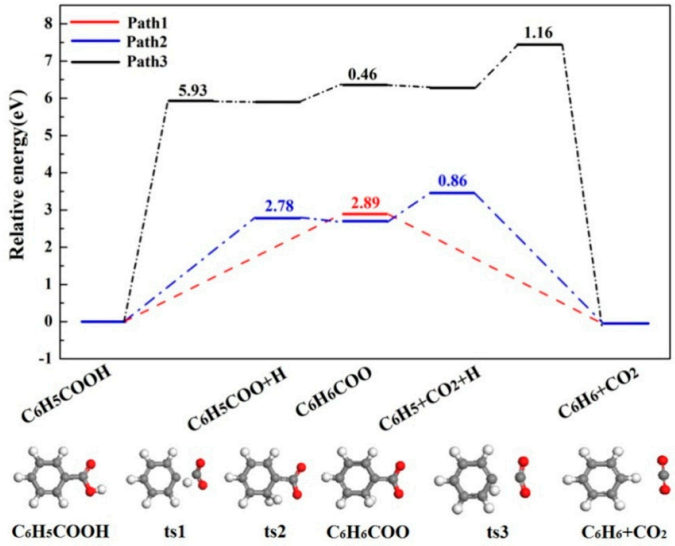

Figure 2. The potential energy diagrams and corresponding IS, TS and FS of C_6H_5COOH pyrolysis.

2.2. Catalytic Pyrolysis

The adsorption structures of possible intermediates of C_6H_5COOH catalytic pyrolysis on Co_3O_4(110)-B, CoO(100) and Co(111) surfaces are shown in Figure 3. The corresponding adsorption energies and geometrical parameters are shown in Table 1.

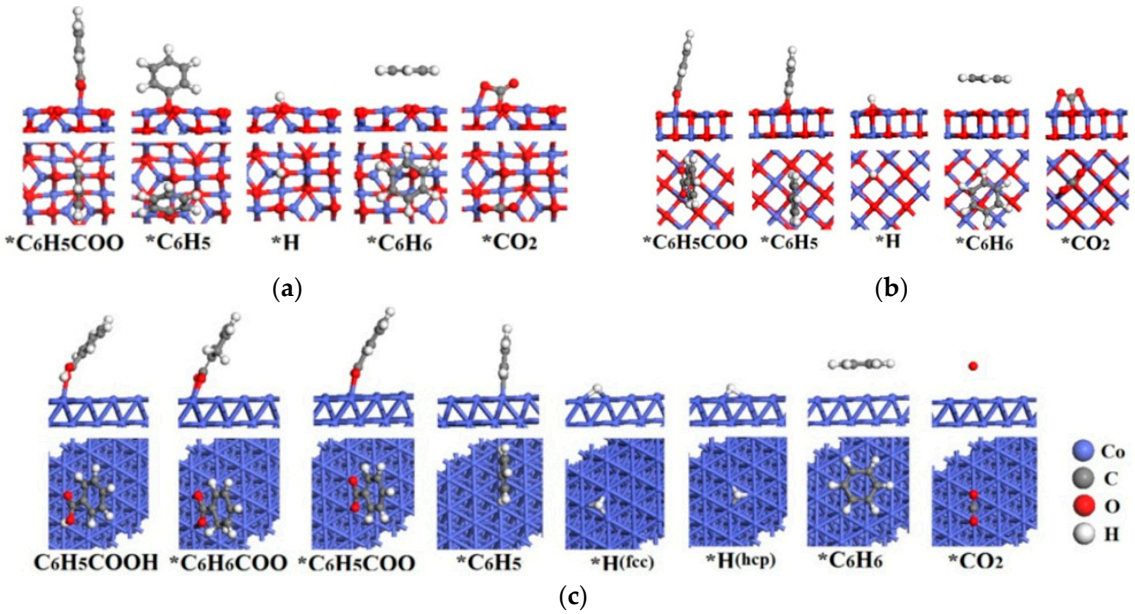

Figure 3. Structures of the possible intermediates of C_6H_5COOH pyrolysis on (**a**) Co_3O_4(110)-B, (**b**) CoO(100) and (**c**) Co(111) surfaces.

Table 1. Adsorption energies and geometrical parameters of relevant species on Co_3O_4(110)-B, CoO(100) and Co(111) surfaces.

Catalysts	Species	Site	E_{ads}(eV)	Bond Length d (Å)
Co_3O_4(110)-B	C_6H_5COO	Co_{oct}	−1.91	$d_{O–Co}$ = 1.835
	C_6H_5	O_{2f}	−3.37	$d_{C–O}$ = 1.362
	H	O_{2f}	−3.59	$d_{H–O}$ = 0.971
	C_6H_6	no bond	−0.01	
	CO_2	O_{2f}, Co_{oct}	−0.64	$d_{C–O}$ = 1.392, $d_{O–Co}$ = 1.954
CoO(100)	C_6H_5COO	Co_{bri}	−3.06	$d_{O–Co}$ = 1.934
	C_6H_5	O_{top}	−2.03	$d_{C–O}$ = 1.387
	H	O_{top}	−2.59	$d_{H–O}$ = 0.976
	C_6H_6	no bond	−0.26	
	CO_2	Co_{top}, O_{top}	−0.40	$d_{C–O}$ = 1.425, $d_{O–Co}$ = 2.107
Co(111)	C_6H_5COOH	top	−0.18	$d_{O–Co}$ = 2.033
	C_6H_6COO	bri	−2.18	$d_{O–Co}$ = 1.956
	C_6H_5COO	bri	−3.08	$d_{O–Co}$ = 1.960
	C_6H_5	top	−2.29	$d_{C–Co}$ = 1.922
	H	fcc	−2.76	$d_{H–Co}$ = 1.622
	H	hcp	−2.73	$d_{H–Co}$ = 1.745
	C_6H_6	no bond	−0.01	
	CO_2	no bond	−0.28	

2.2.1. Co_3O_4(110)-B Surface

The O-H bond scission of $*C_6H_5COOH$ after optimization indicates that C_6H_5COOH is dissociative adsorption on Co_3O_4(110)-B, which is the same as HCOOH adsorption on ZnO surface [28,29], and C_6H_5COOH adsorption on ZnO, MgO, CaO and γ-Al_2O_3 surfaces [20]. $*C_6H_5COO$

adsorbs on Co_{oct} site through one O, the other O points to the adjacent Co_{oct} site with the adsorption energy of −1.91 eV. *H tends to bond with O_{2f} site, which the adsorption energy is −3.59 eV. For $*C_6H_5COO$, the further reaction has two pathways: one is $*C_6H_5COO$ dissociation directly without the assistance of *H ($*C_6H_5COO + *H \rightarrow *C_6H_5 + *CO_2 + *H \rightarrow *C_6H_6 + *CO_2$), and the other is $*C_6H_5COO$ dissociation with *H assistance ($*C_6H_5COO + *H \rightarrow *C_6H_6 + *CO_2$).

For $*C_6H_5COO \rightarrow *C_6H_5 + *CO_2$, the C-C bond length gradually extends from 1.521 Å in the IS to 3.205 Å in the TS. In the FS, $*C_6H_5$ adsorbs on O_{2f} site and $*CO_2$ bonds with O_{2f} and Co_{oct} sites, which the adsorption energies of $*C_6H_5$ and $*CO_2$ are −3.37 and −0.64 eV, respectively. The reaction needs to overcome an energy barrier of 1.88 eV with reaction energy −1.63 eV. Finally, $*C_6H_6$ is formed through $*C_6H_5$ hydrogenation ($*C_6H_5 + *H \rightarrow *C_6H_6$), for which the energy barrier and reaction energy are 2.28 and 1.47 eV. $*C_6H_6$ parallels adsorption on the surface with the adsorption energy of −0.01 eV, which is in accordance with the result calculated by Yildirim [30]. For $*C_6H_5COO + *H \rightarrow *CO_2 + *C_6H_6$, *H bonds with O_{2f} site and $*C_6H_5COO$ adsorbs on Co_{oct} site in the IS. In the TS, the C-C bond length gradually increases to 2.873 Å from 1.517 Å in the IS. The reaction needs to overcome an energy barrier of 2.69 eV with an exothermicity of 0.16 eV.

The potential energy diagrams and corresponding IS, TS and FS geometrical structures of C_6H_5COOH catalytic pyrolysis on Co_3O_4(110)-B surface are shown in Figure 4. It is demonstrated that the energetically preferred pathway of C_6H_5COOH catalytic pyrolysis on Co_3O_4(110)-B is $C_6H_5COOH(g) \rightarrow *C_6H_5COO + *H \rightarrow *C_6H_5 + *CO_2 + *H \rightarrow *CO_2 + *C_6H_6 \rightarrow CO_2(g) + C_6H_6(g)$, which is similar with C_6H_5COOH pyrolysis on MgO, CaO and γ-Al_2O_3 surfaces [20]. The highest energy barrier (2.28 eV) on Co_3O_4(110)-B surface is smaller than that of C_6H_5COOH pyrolysis without a catalyst (2.78 and 2.89 eV). The above results showed that Co_3O_4(110)-B have catalytic effect on C_6H_5COOH pyrolysis.

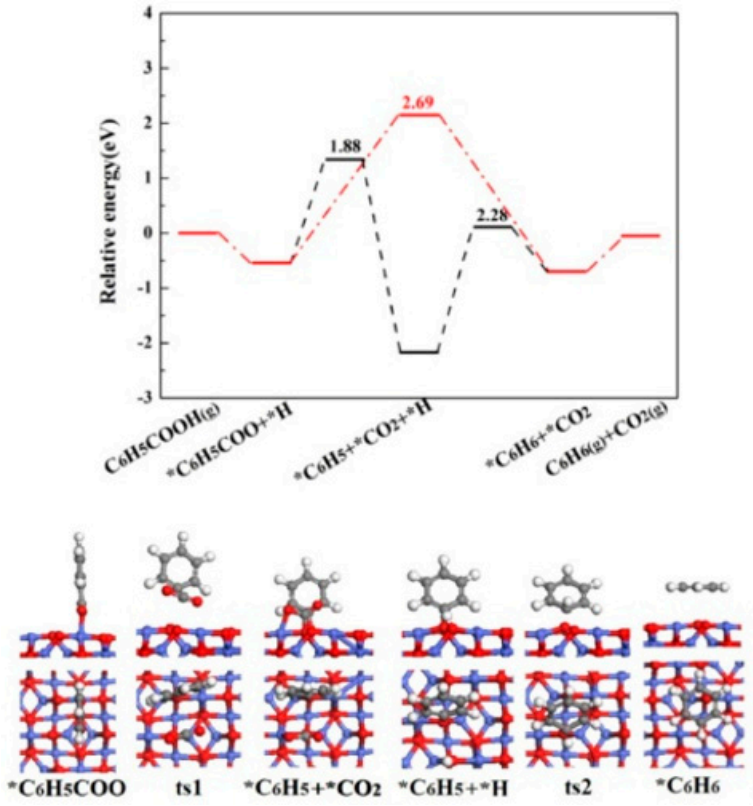

(**a**)

Figure 4. *Cont.*

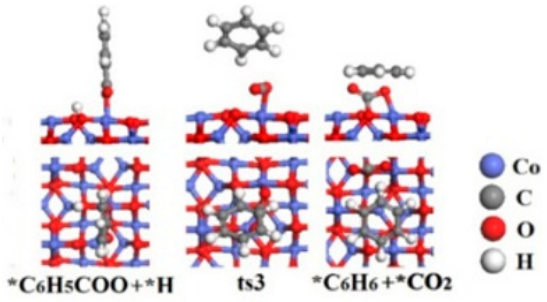

(**b**)

Figure 4. The potential energy diagrams (Red line: $C_6H_5COOH(g) \rightarrow {}^*C_6H_5COO + {}^*H \rightarrow {}^*CO_2 + {}^*C_6H_6 \rightarrow CO_2(g) + C_6H_6(g)$; Black line: $C_6H_5COOH(g) \rightarrow {}^*C_6H_5COO + {}^*H \rightarrow {}^*C_6H_5 + {}^*CO_2 + {}^*H \rightarrow {}^*CO_2 + {}^*C_6H_6 \rightarrow CO_2(g) + C_6H_6(g)$) and corresponding IS, TS and FS geometrical structures of C_6H_5COOH catalytic pyrolysis on Co_3O_4(110)-B surface(**a**) related to black line; (**b**) related to red line.

2.2.2. CoO(100) Surface

$^*C_6H_5COOH$ is also dissociative adsorption on CoO(100) surface after optimization [31]. $^*C_6H_5COO$ binds to Co_{bri} site through two O atoms with the binding energy of −3.06 eV. *H prefers to adsorb on O_{top} site with the adsorption energy of −2.59 eV.

For $^*C_6H_5COO$ dissociation, the C-C bond length gradually increases from 1.497 Å in the IS to 2.798 Å in the TS. The reaction of $^*C_6H_5COO \rightarrow {}^*C_6H_5 + {}^*CO_2$ overcomes an energy barrier of 1.70 eV with reaction energy 1.21 eV. $^*C_6H_5$ tends to bond with O_{top} site via ipso-C, which the adsorption energy is −2.03 eV. $^*CO_2$ bonds with O_{top} and Co_{top} sites with the binding energy of −0.40 eV. The energy barrier and reaction energy of $^*C_6H_5$ hydrogenation ($^*C_6H_5 + {}^*H \rightarrow {}^*C_6H_6$) are 2.01 and −1.12 eV. $^*C_6H_6$ is the parallel adsorption on the surface with the adsorption energy of −0.26 eV. With H assistance, the process of $^*C_6H_5COO + {}^*H \rightarrow {}^*CO_2 + {}^*C_6H_6$ needs to overcome the energy barrier of 0.82 eV with the reaction energy of 0.09 eV.

The potential energy diagrams and corresponding IS, TS and FS geometrical structures of C_6H_5COOH catalytic pyrolysis on CoO(100) surface are shown in Figure 5. As shown in Figure 5, the energetically preferred pathway of C_6H_5COOH catalytic pyrolysis on CoO(100) is $C_6H_5COOH(g) \rightarrow {}^*C_6H_5COO + {}^*H \rightarrow {}^*CO_2 + {}^*C_6H_6 \rightarrow CO_2(g) + C_6H_6(g)$. The highest energy barrier (2.01 eV) on CoO(100) surface is also smaller than that of C_6H_5COOH pyrolysis (2.78 and 2.89 eV), showing that CoO(100) surface exhibits a catalytic effect on C_6H_5COOH decomposition. C_6H_5COOH catalytic pyrolysis pathway on CoO(100) surface is same as on ZnO [20], but is different on Co_3O_4(110)-B surface.

2.2.3. Co(111) Surface

On Co(111) surface, $^*C_6H_5COOH$ binds to top site via O atom, and the adsorption energy is −0.18 eV. The result shows that $^*C_6H_5COOH$ on Co(111) surface uses nondissociation adsorption, which is different from $^*C_6H_5COOH$ adsorption on CoO(100) and Co_3O_4(110)-B surface. There are three possible pathways for $^*C_6H_5COOH$ further reaction: the first is $^*C_6H_6$ and $^*CO_2$ formation ($^*C_6H_5COOH \rightarrow {}^*C_6H_6 + {}^*CO_2$), the second is the formation of $^*C_6H_6COO$ ($^*C_6H_5COOH \rightarrow {}^*C_6H_6COO$) and the third is $^*C_6H_5COOH$ dehydrogenation ($^*C_6H_5COOH \rightarrow {}^*C_6H_5COO + {}^*H$).

The energy barrier and reaction energy of $^*C_6H_5COOH \rightarrow {}^*C_6H_6 + {}^*CO_2$ are 6.10 and −0.16 eV. $^*C_6H_6$ and CO_2 are parallel adsorption on the surface, and the corresponding adsorption energies are −0.01 and −0.28 eV. For the reaction of $^*C_6H_5COOH \rightarrow {}^*C_6H_6COO$, the process overcomes an energy barrier of 8.68 eV with an endothermicity of 0.71 eV. $^*C_6H_6COO$ prefers to bind at a bridge site through O atoms with an adsorption energy of −2.18 eV. However, the energy barrier of $^*C_6H_5COOH \rightarrow {}^*C_6H_5COO + {}^*H$ is 4.99 eV, which is far smaller than that of $^*C_6H_5COOH \rightarrow {}^*C_6H_6 + {}^*CO_2$ and $^*C_6H_5COOH \rightarrow {}^*C_6H_6COO$. The result shows that $^*C_6H_5COOH$ dehydrogenation is the most favorable pathway for $^*C_6H_5COOH$ further reaction. The adsorption sites of *H are fcc and hcp sites, which

the adsorption energies are −2.76 and −2.73 eV, respectively. The calculation result is consistent with the results of Chen et al. [32]. C_6H_5COO adsorbs strongly at the bridge site, for which the adsorption energy is −3.08 eV.

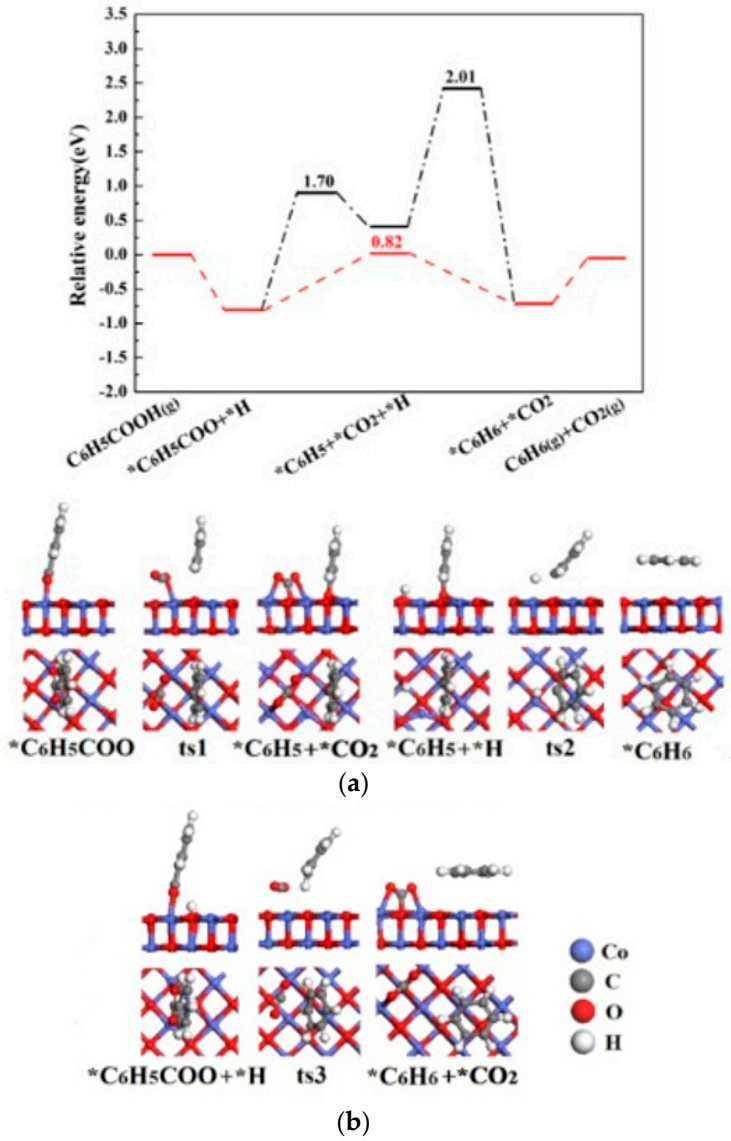

Figure 5. The potential energy diagrams (Red line: $C_6H_5COOH(g) \rightarrow {}^*C_6H_5COO + {}^*H \rightarrow {}^*CO_2 + {}^*C_6H_6 \rightarrow CO_2(g) + C_6H_6(g)$; Black line:$C_6H_5COOH(g) \rightarrow {}^*C_6H_5COO + {}^*H \rightarrow {}^*C_6H_5 + {}^*CO_2 + {}^*H \rightarrow {}^*CO_2 + {}^*C_6H_6 \rightarrow CO_2(g) + C_6H_6(g)$) and corresponding IS, TS, and FS geometrical structures of C_6H_5COOH catalytic pyrolysis on CoO(100) surface (**a**) related to black line; (**b**) related to red line.

Similarity of C_6H_5COO dissociation on Co_3O_4(110)-B and CoO(100) surfaces, there are also two possible pathways on Co(111): one is the formation of $^*C_6H_5$ and $^*CO_2$ without *H assistance, for which the energy barrier and reaction energy are 2.77 and 0.99 eV. $^*C_6H_5$ adsorbs on the top site via ipso-C with the adsorption energy of −2.29 eV. Then, $^*C_6H_6$ is formed by $^*C_6H_5$ hydrogenation (E_a = 3.84 eV, $\Delta H = -0.45$ eV). The other is $^*C_6H_6$ and $^*CO_2$ formation with *H assistance, for which the energy barrier and reaction energy are 2.39 and 0.54 eV.

Figure 6 shows the potential energy diagrams and corresponding IS, TS and FS geometrical structures of C_6H_5COOH catalytic pyrolysis on Co(111) surface. It is demonstrated that the energetically preferred pathway of C_6H_5COOH catalytic pyrolysis on Co(111) surface is $C_6H_5COOH(g) \rightarrow {}^*C_6H_5COOH \rightarrow {}^*C_6H_5COO + {}^*H \rightarrow {}^*CO_2 + {}^*C_6H_6 \rightarrow CO_2(g) + C_6H_6(g)$. The highest energy

barrier (4.99 eV) of C_6H_5COOH catalytic pyrolysis on Co(111) surface is greater than that without catalysts (2.78 and 2.89 eV), indicating that Co(111) surface does not show catalytic effect on C_6H_5COOH pyrolysis.

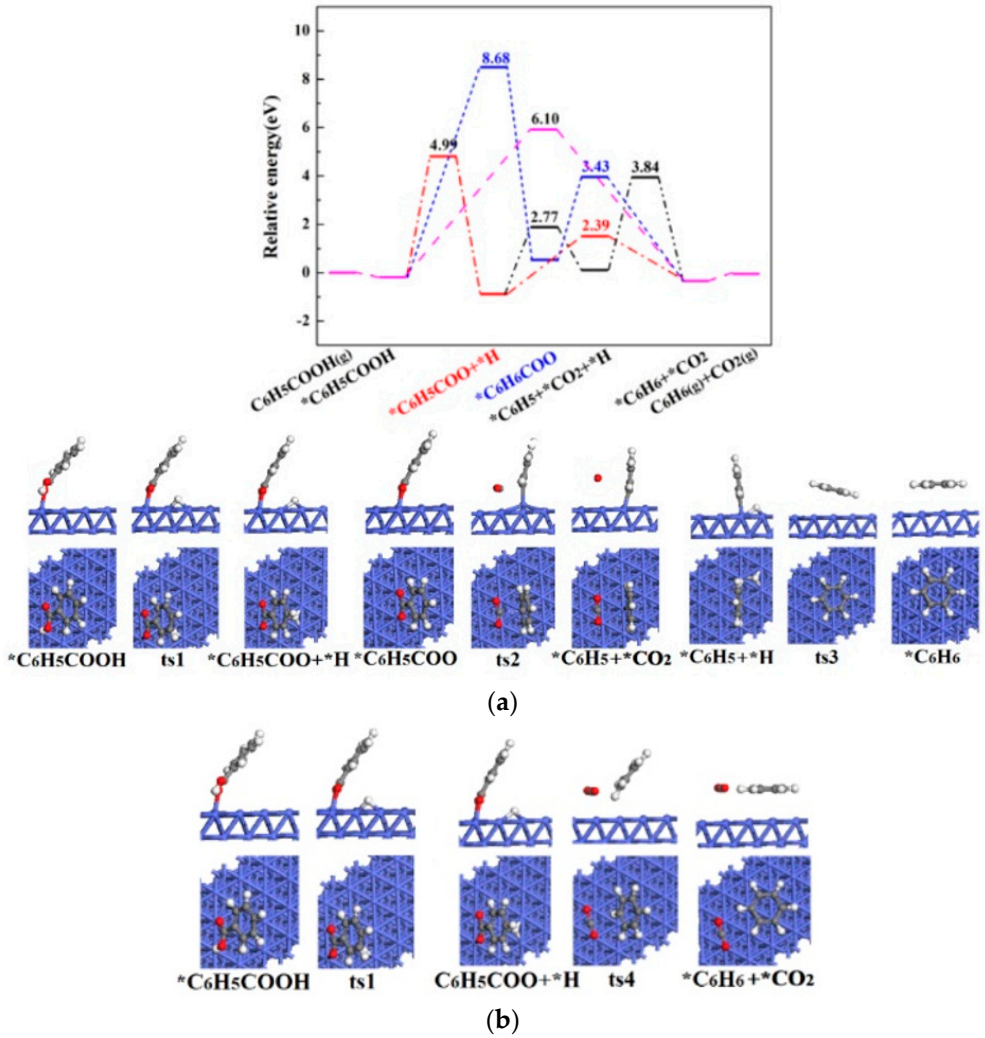

Figure 6. The potential energy diagrams (Purple line: $C_6H_5COOH(g) \rightarrow *C_6H_5COOH \rightarrow *C_6H_6 + *CO_2 \rightarrow C_6H_6(g) + CO_2(g)$; Blue line: $C_6H_5COOH(g) \rightarrow *C_6H_5COOH \rightarrow *C_6H_6COO \rightarrow *C_6H_6 + *CO_2 \rightarrow C_6H_6(g) + CO_2(g)$; Red line: $C_6H_5COOH(g) \rightarrow *C_6H_5COOH \rightarrow *C_6H_5COO + *H \rightarrow *C_6H_6 + *CO_2 \rightarrow C_6H_6(g) + CO_2(g)$; Black line: $C_6H_5COOH(g) \rightarrow *C_6H_5COOH \rightarrow *C_6H_5COO + *H \rightarrow *C_6H_5 + *CO_2 + *H \rightarrow *C_6H_6 + *CO_2 \rightarrow C_6H_6(g) + CO_2(g)$) and corresponding IS, TS and FS geometrical structures of C_6H_5COOH catalytic pyrolysis on Co(111) surface (**a**) related to black line; (**b**) related to red line.

2.3. d-band Center Analyses

The calculation of d-band center is based on all cobalt atoms to each surface. The corresponding d-band centers of Co_3O_4(110)-B, CoO(100) and Co(111) are −4.32, −2.35 and −1.42 eV relative to the Fermi level, respectively. The highest energy barriers of C_6H_5COOH catalytic pyrolysis on Co_3O_4(110)-B, CoO(100) and Co(111) are 2.28, 0.82, and 4.99 eV, respectively. It is found that there is a volcano-like relationship between d-band center and the highest energy barrier [33].

3. Computational Methods and Models

DFT calculations were carried out with the Vienna ab initio simulation package (VASP) [34,35]. The projector-augmented-wave (PAW) potentials were employed to calculate the interaction

between ion core and valence electron [36]. The Perdew−Burke−Ernzerh (PBE) [37] generalized gradient approximation (GGA) [38] functional was performed to describe electronic structure [37]. The climbing-image nudged-elastic-band method (CI-NEB) was applied to derive the transition states (TS) [39], which was confirmed by one imaginary frequency. 3 × 3 × 1 k-points and the cutoff energy with 415 eV were used.

Co_3O_4(110)-B, CoO(100) and Co(111) surfaces were modeled with (2 × 1), (3 × 4) and (4 × 6) supercells separated by a 15 Å vacuum. The bottom two layers were fixed while other layers and the adsorbates were relaxed during the geometry optimization. Co^{2+} and Co^{3+} of Co_3O_4(110)-B both are antimagnetic [40], which the magnetic moments were set to 2.53 and 2.44 μB, respectively. For CoO(100), the magnetic moment of Co^{2+} was set to 2.64 μB [41]. The DFT+U method [42–44] was performed to Co_3O_4(110)-B and CoO(100) surfaces because of the error caused by 3d-oribit spin in the Co atoms. The U_{eff}=U-J values of Co_3O_4(110)-B and CoO(100) were set to 2.0 and 3.3 eV, respectively. The surface energies of the three surfaces with different numbers of layers are shown in Table 2. According to Table 2, a four-layer slab, a five-layer slab and a four-layer slab for Co_3O_4(110)-B, CoO(100) and Co(111) surfaces were used. Top and side views of three surfaces are shown in Figure 7.

Table 2. The surface energies of Co_3O_4(110)-B, CoO(100) and Co(111) surfaces.

Catalysts	Number of Layers	Surface Energies(J/m^2)
Co_3O_4(110)-B	4	1.24
	6	1.22
CoO(100)	5	0.54
	6	0.52
Co(111)	3	1.84
	4	1.78
	5	1.76

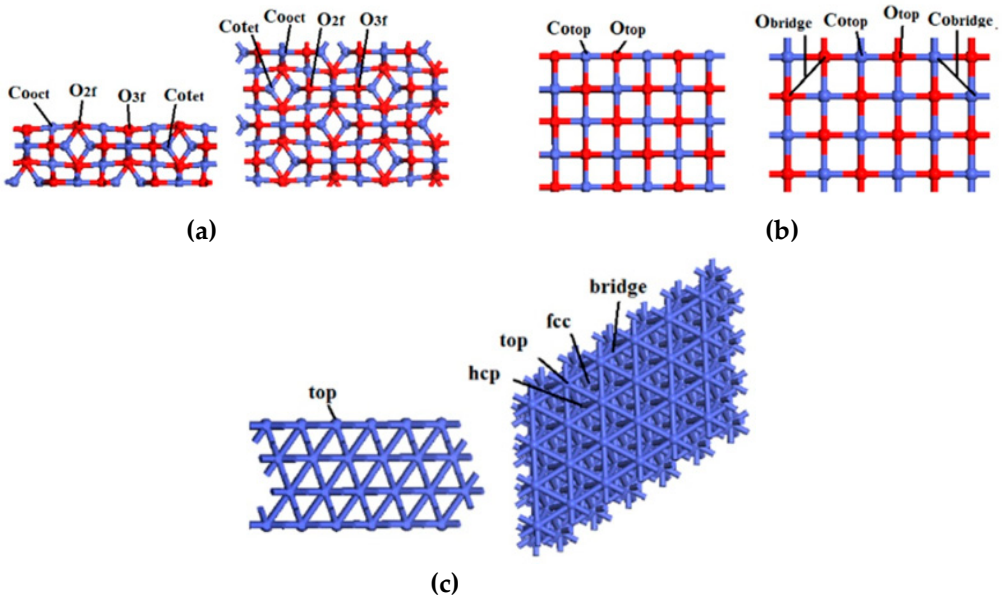

Figure 7. The top and side views of (**a**) Co_3O_4(110)-B, (**b**) CoO(100) and (**c**) Co(111) surfaces.

4. Conclusions

In this study, during the pyrolysis of C_6H_5COOH, the effect of the valence state change of cobalt oxides is investigated with the DFT method. Based on the calculated results, there are two possible pathways for C_6H_5COOH pyrolysis without catalyst: one is $C_6H_5COOH \rightarrow CO_2 + C_6H_6$; the other is $C_6H_5COOH \rightarrow C_6H_6COO \rightarrow CO_2 + C_6H_6$. There are three possibilities for C_6H_5COOH pyrolysis with catalyst. On Co_3O_4(110)-B surface, the energetically preferred pathway is C_6H_5COOH(g)

$\rightarrow$*C_6H_5COO + *H $\rightarrow$ *CO_2 + *C_6H_5 + *H $\rightarrow$ *CO_2 + *C_6H_6 $\rightarrow$$CO_2$(g) + C_6H_6(g). On CoO(100) surface, the energetically preferred pathway is C_6H_5COOH(g) $\rightarrow$*C_6H_5COO + *H $\rightarrow$ *CO_2 + *$C_6H_6$$\rightarrow$$CO_2$(g) + C_6H_6(g). On Co(111) surface, the energetically preferred pathway is C_6H_5COOH(g) $\rightarrow$*C_6H_5COOH $\rightarrow$*C_6H_5COO + *H $\rightarrow$ *CO_2 + *$C_6H_6$$\rightarrow$$CO_2$(g) + C_6H_6(g). Compared with the highest energy barrier of C_6H_5COOH pyrolysis, it is found in the following order: E_a(CoO) <E_a(Co_3O_4) <E_a(no catalyst) <E_a(Co). The above results showed that the presence of catalysts could change the reaction pathway and energy barrier. Co_3O_4 and CoO can promote C_6H_5COOH pyrolysis, and the catalytic effect of CoO is much more effective. However, metallic Co does not show catalytic effect on the C_6H_5COOH pyrolysis. In short, cobalt oxides improve the catalytic activity of C_6H_5COOH pyrolysis, but catalysis does not occur when cobalt oxides are reduced as metallic Co.

Author Contributions: S.-M.F. and J.-T.L. carried out the research; Y.Z. wrote the paper; W.-S.L. and G.-S.L. prepared the paper; W.H. and Z.-J.Z. revised the paper.

Funding: This work was financially supported by the National Natural Science Foundation of China (21776197 and 21776195) and Shanxi Province Science Foundation for Youths (201701D211003).

Conflicts of Interest: The authors declare no conflicts of interest.

References

1. Liu, L.L.; Kumar, S.; Wang, Z.H.; He, Y.; Liu, J.Z.; Cen, K. Catalytic Effect of Metal Chlorides on Coal Pyrolysis and Gasification Part I. Combined TG-FTIR Study for Coal Pyrolysis. *Thermochim. Acta* **2017**, *655*, 331–336. [CrossRef]
2. Hu, H.Q.; Zhou, Q.; Zhu, S.W.; Meyer, B.; Krzack, S.; Chen, G.H. Product distribution and sulfur behavior in coal pyrolysis. *Fuel Process. Technol.* **2004**, *85*, 849–861. [CrossRef]
3. Solomon, P.R.; Serio, M.A.; Suuberg, E.M. Coal pyrolysis: Experiments, kinetic rates and mechanisms. *Prog. Energy Combust. Sci.* **1992**, *18*, 133–220. [CrossRef]
4. Zarnegar, S. A review on catalytic pyrolysis of coal and biomass for value added fuel and chemicals. *Energy Sources Part A Recover. Util. Environ. Eff.* **2018**, *40*, 1427–1433. [CrossRef]
5. Wang, X.J.; Zhu, H.L.; Wang, X.M.; Liu, H.F.; Wang, F.C.; Yu, G.S. Transformation and Reactivity of a Potassium Catalyst during Coal–Steam Catalytic Pyrolysis and Gasification. *Energy Technol.* **2014**, *2*, 598–603. [CrossRef]
6. Fu, Y.; Guo, Y.H.; Zhang, K.X. Effect of Three Different Catalysts (KCl, CaO, and Fe_2O_3) on the Reactivity and Mechanism of Low-Rank Coal Pyrolysis. *Energy Fuels* **2016**, *30*, 2428–2433. [CrossRef]
7. Lei, Z.; Sha, X.L.; Lei, Z.; Wang, R.; Zhang, L.X.; Shu, X.Q. Influences of Different Preparation Conditions on Catalytic Activity of Ag_2O-Co_3O_4/γ-$Al_2O_3$for Hydrogenation of Coal Pyrolysis. *J. Spectrosc.* **2014**, *2014*, 1–6.
8. Yan, S.; Zhang, J.S.; Yan, X.Q.; Pan, D.F.; Ren, H.; Qu, X. Catalytic coal hydrogasification by cobalt-calcium catalyst in a pressurized fluidized bed: Role of hydropyrolysis and catalysis process. *J. Anal. Appl. Pyrolysis* **2018**, *135*, 251–259. [CrossRef]
9. Liang, L.T.; Huai, J.T.; Zhang, Q.; Liu, J.W.; Huang, W.; Zhang, Z.L.; Hao, X.G.; Guan, G.Q. Catalytic depolymerization of a typical lignite for improving tar yield by Co and Zn catalyst. *Sci. Rep.* **2017**, *7*, 14433. [CrossRef]
10. Takarada, T.; Onoyama, Y.; Takayama, K.; Sakashita, T. Hydropyrolysis of coal in a pressurized powder-particle fluidized bed using several catalysts. *Catal. Today* **1997**, *39*, 127–136. [CrossRef]
11. Li, G.; Li, L.; Shi, L.; Jin, L.J.; Tang, Z.C.; Fan, H.J.; Hu, H.Q. Experimental and Theoretical Study on the Pyrolysis Mechanism of Three Coal-Based Model Compounds. *Energy Fuels* **2014**, *28*, 980–986. [CrossRef]
12. Liu, S.Y.; Zhang, Z.Q.; Wang, H.F. Quantum chemical investigation of the thermal pyrolysis reactions of the carboxylic group in a brown coal model. *J. Mol. Model.* **2012**, *18*, 359–365. [CrossRef] [PubMed]
13. Murata, S.; Hosokawa, M.; Kidena, K.; Nomura, M. Analysis ofoxygen-functional groups in brown coals. *Fuel Process. Technol.* **2000**, *67*, 231–243. [CrossRef]
14. Li, L.; Fan, H.J.; Hu, H.Q. A theoretical study on bond dissociation enthalpies of coal based model compounds. *Fuel* **2015**, *153*, 70–77. [CrossRef]
15. Li, J.; Zhang, F.; Fang, W.H. Probing Photophysical and Photochemical Processes of Benzoic Acid from ab Initio Calculations. *J. Phys. Chem. A* **2005**, *109*, 7718–7724. [CrossRef] [PubMed]

16. Wu, J.H.; Wang, J.; Liu, J.Z.; Yang, Y.M.; Cheng, J.; Wang, Z.H.; Zhou, J.H.; Cen, K.F. Moisture removal mechanism of low-rank coal by hydrothermal dewatering: Physicochemical property analysis and DFT calculation. *Fuel* **2017**, *187*, 242–249. [CrossRef]
17. Li, B.; Liu, S.Y.; Guo, J.Y.; Zhang, L. Interaction between low rank coal and kaolinite particles: A DFT simulation. *Appl. Surf. Sci.* **2018**, *456*, 215–220. [CrossRef]
18. Kong, L.H.; Li, G.; Jin, L.J.; Hu, H.Q. Pyrolysis behaviors of two coal-related model compounds on a fixed-bed reactor. *Fuel Process. Technol.* **2015**, *129*, 113–119. [CrossRef]
19. Gao, M.J.; Li, X.X.; Guo, L. Pyrolysis simulations of Fugu coal by large-scale ReaxFF molecular dynamics. *Fuel Process. Technol.* **2018**, *178*, 197–205. [CrossRef]
20. Wang, M.F.; Zuo, Z.J.; Ren, R.P.; Gao, Z.H.; Huang, W. Theoretical Study on Catalytic Pyrolysis of Benzoic Acid as a Coal-Based Model Compound. *Energy Fuels* **2016**, *30*, 2833–2840. [CrossRef]
21. Cui, L.P.; Liu, J.T.; Liu, S.Z.; Wang, M.F.; Gao, Z.H.; Zuo, Z.J.; Huang, W. A DFT study of the catalytic pyrolysis of benzaldehyde on ZnO, γ-Al_2O_3. *J. Mol. Model.* **2018**, *24*, 65. [CrossRef] [PubMed]
22. Liu, J.T.; Wang, M.F.; Gao, Z.H.; Zuo, Z.J.; Huang, W. The role of catalysts in the decomposition of phenoxy compounds in coal: A density functional theory study. *Appl. Surf. Sci.* **2018**, *428*, 541–548. [CrossRef]
23. Wang, B.W.; Liu, S.H.; Hu, Z.Y.; Li, Z.H.; Ma, X.B. Active phase of highly active Co_3O_4 catalyst for synthetic natural gas production. *RSC Adv.* **2014**, *4*, 57185–57191. [CrossRef]
24. Garces, L.J.; Hincapie, B.; Zerger, R.; Suib, S.L. The Effect of Temperature and Support on the Reduction of Cobalt Oxide: An in Situ X-ray Diffraction Study. *J. Phys. Chem. C* **2015**, *119*, 5484–5490. [CrossRef]
25. Manion, J.A.; McMillen, D.F.; Malhotra, R. Decarboxylation and coupling reactions of aromatic acids under coal-liquefaction conditions. *Energy Fuels* **1996**, *10*, 776–788. [CrossRef]
26. Eskay, T.P.; Britt, P.F.; Buchanan, A.C., III. Does Decarboxylation Lead to Cross-Linking in Low-Rank Coals? *Energy Fuels* **1996**, *10*, 1257–1261. [CrossRef]
27. Eskay, T.P.; Britt, P.F.; Buchanan, A.C., III. *Pyrolysis of Coal Model Compounds Containing Aromatic Carboxylic Acids: The Role of Carboxylic Acids in Cross-Linking Reactions in Low-Rank Coal*; Oak Ridge National Lab.: Oak Ridge, TN, USA, 1997.
28. Labat, F.; Ciofini, I.; Adamo, C. Modeling ZnO phases using a periodic approach: From bulk to surface and beyond. *J. Chem. Phys.* **2009**, *131*, 044708. [CrossRef] [PubMed]
29. Buchholz, M.; Li, Q.; Noei, H.; Nefedov, A.; Wang, Y.M.; Muhler, M.; Fink, K.; Wöll, C. The Interaction of Formic Acid with Zinc Oxide: A Combined Experimental and Theoretical Study on Single Crystal and Powder Samples. *Top. Catal.* **2015**, *58*, 174–183. [CrossRef]
30. Yildirim, H.; Greber, T.; Kara, A. Trends in Adsorption Characteristics of Benzene on Transition Metal Surfaces: Role of Surface Chemistry and van der Waals Interactions. *J. Phys. Chem. C* **2013**, *117*, 20572–20583. [CrossRef]
31. Schwarz, M.; Hohner, C.; Mohr, S.; Libuda, J. Dissociative Adsorption of Benzoic Acid on Well-Ordered Cobalt Oxide Surfaces: Role of the Protons. *J. Phys. Chem. C* **2017**, *121*, 28317–28327. [CrossRef]
32. Chen, C.B.; Wang, Q.; Wang, G.R.; Hou, B.; Jia, L.T.; Li, D.B. Mechanistic Insight into the C_2 Hydrocarbons Formation from Syngas on fcc-Co(111) Surface: A DFT Study. *J. Phys. Chem. C* **2016**, *120*, 9132–9147. [CrossRef]
33. Kuttiyiel, K.A.; Choi, Y.; Hwang, S.M.; Park, G.G.; Yang, T.H.; Su, D.; Sasaki, K.; Liu, P.; Adzic, R.R. Enhancement of the oxygen reduction on nitride stabilized pt-M (M=Fe, Co, and Ni) core–shell nanoparticle electrocatalysts. *Nano Energy* **2015**, *13*, 442–449. [CrossRef]
34. Kresse, G.; Furthmüller, J. Efficient iterative schemes for ab initio total-energy calculations using a plane-wave basis set. *Phys. Rev. B* **1996**, *54*, 11169. [CrossRef]
35. Kresse, G.; Furthmüller, J. Efficiency of ab-initio total energy calculations for metals and semiconductors using a plane-wave basis set. *Comput. Mater. Sci.* **1996**, *6*, 15–50. [CrossRef]
36. Kresse, G.; Joubert, D. From ultrasoft pseudopotentials to the projector augmented-wave method. *Phys. Rev. B* **1999**, *59*, 1758. [CrossRef]
37. Blöchl, P.E. Projector augmented-wave method. *Phy. Rev. B* **1994**, *50*, 17953. [CrossRef]
38. Perdew, J.P.; Burke, K.; Ernzerhof, M. Generalized Gradient Approximation Made Simple. *Phys. Rev. Lett.* **1996**, *77*, 3865. [CrossRef] [PubMed]
39. Sheppard, D.; Xiao, P.H.; Chemelewski, W.; Johnson, D.D.; Henkelman, G. A generalized solid-state nudged elastic band method. *J. Chem. Phys.* **2012**, *136*, 074103. [CrossRef] [PubMed]

40. Hu, W.; Lan, J.; Guo, Y.; Cao, X.M.; Hu, P. Origin of Efficient Catalytic Combustion of Methane over Co_3O_4(110) Active Low-Coordination Lattice Oxygen and Cooperation of Multiple Active Sites. *ACS Catal.* **2016**, *6*, 5508–5519. [CrossRef]
41. Shojaee, K.; Haynes, B.S.; Montoya, A. Molecular modelling of the decomposition of NH_3 over CoO(100). *Mater. Chem. Phys.* **2015**, *156*, 141–149. [CrossRef]
42. Selcuk, S.; Selloni, A. DFT+U Study of the Surface Structure and Stability of Co_3O_4(110): Dependence on U. *J. Phys. Chem. C* **2015**, *119*, 9973–9979. [CrossRef]
43. Wang, L.; Maxisch, T.; Ceder, G. Oxidation energies of transition metal oxides within the GGA+U framework. *Phys. Rev. B* **2006**, *73*, 195107. [CrossRef]
44. Dudarev, S.L.; Botton, G.A.; Savrasov, S.Y.; Humphreys, C.J.; Sutton, A.P. Electron-energy-loss spectra and the structural stability of nickel oxide: An LSDA+U study. *Phys. Rev. B* **1998**, *57*, 1505. [CrossRef]